RSC Advances

PAPER

Cite this: *RSC Adv.*, 2024, **14**, 16240

AC conductivity study of mechanochemically synthesized solid electrolytes of $Li_{6-a}M_{a/n}{}^{n}PS_5Cl$ (M = Ca, Mg, Ba, Zn, Al, Y)†

Tran Viet Toan,[ab] Luu Tuan Anh,[ab] Nguyen Thi Minh Nguyet,[bc] Tran Anh Tu[abd] and Nguyen Huu Huy Phuc *[abd]

Received 8th April 2024
Accepted 16th May 2024

DOI: 10.1039/d4ra02621g

rsc.li/rsc-advances

Argyrodite-type solid electrolytes of Li_6PS_5Cl doped with multivalent cations (Mg^{2+}, Ba^{2+}, Zn^{2+}, Al^{3+}, Y^{3+}) were prepared *via* a mechanochemical synthesis method. The lattice constant (a_0), interplanar spacing (d_{220}, d_{311}, d_{222}), and micro-strain (ε) showed that the doping elements were incorporated into the crystal structure of Li_6PS_5Cl. The lattice constant and interplanar spacing of the doped samples were smaller than those of Li_6PS_5Cl. The prepared samples exhibited a positive lattice strain, and the substituted samples exhibited higher strains than Li_6PS_5Cl. The doped samples exhibited higher ionic conductivity than Li_6PS_5Cl at 25 °C. $Li_{5.94}Al_{0.02}PS_5Cl$ exhibited the highest σ_{DC} of approximately 2.36 × 10^{-3} S cm^{-1} at 25 °C. The charge carrier movement at the grain boundary changing from long-range diffusion in Li_6PS_5Cl to short-range diffusion in $Li_{5.94}Al_{0.02}PS_5Cl$ enhanced the conductivity.

1. Introduction

All-solid-state Li ion batteries using sulfide-based solid electrolytes (SEs) are candidates for technological applications because of their high energy density, thermal stability, and ease of cell design.[1] SEs with high ionic conductivity at 25 °C are important components of all-solid-state Li ion batteries. $Li_7P_3S_{11}$, $Li_{10}GeP_2S_{12}$, $Li_{10}P_3S_{12}I$, and argyrodite-type Li_6PS_5Cl SEs have attracted considerable attention from researchers because of their tunable composition and attractive ionic conductivity at 25 °C.[2–5] Argyrodite-type SEs have been intensively studied because they have a wide electrochemical window and exhibit high ionic conductivity.[6]

The ionic conductivity of Li_6PS_5X (X = Cl, Br, and I) at room temperature ranges from 10^{-6} to approximately 1–2 × 10^{-3} S cm^{-1} and could be improved by the aliovalent substitution of S^{2-}, P^{5+}, and Li^+. $Li_{5.5}PS_{4.5}Cl_{1.5}$ exhibited a high conductivity of 9.4 × 10^{-3} S cm^{-1} at 25 °C,[7] whereas $Li_{5.3}PS_{4.3}Cl_{1.0}Br_{0.7}$ exhibited an ionic conductivity of 16.6 × 10^{-3} S cm^{-1} at 30 °C.[8] High-entropy multicationic substituted $Li_{6.5}[P_{0.25}Si_{0.25}Ge_{0.25}Sb_{0.25}]S_5I$ exhibited a high ionic conductivity of approximately 13 × 10^{-3} S cm^{-1} at room temperature,[9] and $Li_{6.2}Si_{0.2}P_{0.8}S_5Cl_{0.5}Br_{0.5}$ exhibited a high ionic conductivity of 5.12 × 10^{-3} S cm^{-1} at room temperature.[10] The aliovalent substitution of Li^+ by a multivalent cation improved the ionic conductivity of Li_6PS_5Cl. The ionic conductivity of $Li_{5.7}Ca_{0.15}PS_5Cl$ at 25 °C was approximately 5.2 × 10^{-3} S cm^{-1}, which exceeded that of Li_6PS_5Cl (3.1 × 10^{-3} S cm^{-1}).[11] $Li_{5.4}Al_{0.2}PS_5Br$ exhibited a room temperature ionic conductivity of 2.4 × 10^{-3} S cm^{-1}, which exceeded that of Li_6PS_5Br (1.0 × 10^{-3} S cm^{-1}).[12] These SEs were prepared through solid-state reactions at a high temperature. Therefore, maintaining low oxygen and humidity concentrations will be a barrier to the mass production of these substances because sulfide-based SEs react with oxygen in a dry atmosphere at approximately 270 °C.[13] Thus, mechanochemical synthesis, which occurs at room temperature, is a good option, in addition to solid-state reactions at high temperatures. The ionic conductivity of mechanochemically synthesized Li_6PS_5Cl at room temperature was slightly enhanced because of a multivalent cation at the grain boundary.[14]

This study enhanced the ionic conductivity of mechanochemically synthesized Li_6PS_5Cl by the aliovalent substitution of Li^+ with multivalent cations (Mg^{2+}, Ba^{2+}, Zn^{2+}, Al^{3+}, Y^{3+}). Data obtained from alternating current (AC) impedance spectroscopy was analyzed using conductivity isotherms and the dielectric constant and dielectric loss. The ionic conductivity of $Li_{5.94}Al_{0.02}PS_5Cl$ was approximately 2.36 × 10^{-3} S cm^{-1} at 25 °C, which was approximately twice that of Li_6PS_5Cl. Furthermore, this value exceeded the reported ionic conductivity of argyrodite SEs prepared without heat treatment. The activation energy of direct current and Li ion migration suggested that ion movement at the grain boundary was a critical process in the prepared samples.

[a]Faculty of Materials Technology, Ho Chi Minh City University of Technology (HCMUT), 268 Ly Thuong Kiet Str., Dist. 10, Ho Chi Minh City, Vietnam. E-mail: nhhphuc@hcmut.edu.vn

[b]Vietnam National University Ho Chi Minh City, Linh Trung Ward, Thu Duc Dist., Ho Chi Minh City, Vietnam

[c]VNU-HCM Key Laboratory for Material Technologies, Ho Chi Minh City University of Technology (HCMUT), 268 Ly Thuong Kiet Str., Dist. 10, Ho Chi Minh City, Vietnam

[d]National Key Laboratory of Polymer and Composite Materials – Ho Chi Minh City, 268 Ly Thuong Kiet, District 10, Ho Chi Minh City, Vietnam

† Electronic supplementary information (ESI) available. See DOI: https://doi.org/10.1039/d4ra02621g

2. Experimental process

The samples were prepared *via* a mechanical milling synthesis method. Li_2S, P_2S_5, LiCl, $CaCl_2$, $BaCl_2$, $MgCl_2$, YCl_3, $AlCl_3$, and $ZnCl_2$ were obtained from Macklin at 99.9% purity and used without further purification. A typical batch (2.000 g) was prepared by mixing an appropriate amount of each starting material using agar and a mortar for approximately 15 min. The mixture was transferred into a zirconia pot (45 mL) with zirconia balls (approximately 30 g; diameter = 5 mm). The ball-to-powder ratio was approximately 15. The pot was rotated at 550 rpm for 20 h using a Pulverisette 7 (Fritsch Co., Ltd). The samples were recovered and characterized without further heat treatment. All the synthesis experiments were performed in a dry Ar atmosphere.

The structure of the samples was characterized by X-ray diffraction (XRD; X8, Bruker), SEM (S4800, Hitachi) and EDS (ULTIM MAX, Oxford Instrument). The samples were prepared in an Ar-filled glove box and loaded into an air-tight sample holder for characterization.

The samples for resistivity measurements were prepared by uniaxially cold pressing the powder under a pressure of 330 MPa to form a pellet (thickness = 1.2–1.4 mm; diameter = 10 mm), as reported.[15] AC impedance spectroscopy was conducted using a potentiostat (PGSTAT302N, Autolab, Herisau, Switzerland) from 9 MHz to 10 Hz. The samples for the impedance measurements were prepared by uniaxially pressing the sample (approximately 160 mg) into pellets (approximately 10.0 mm in diameter) under a pressure of 330 MPa at room temperature. The pellet was placed in a holder made of polycarbonate with two stainless steel rods as blocking electrodes. Thereafter, the cell was placed in an N_2 flow in a glass tube for temperature dependence measurements. The temperature was gradually increased from room temperature to 110 °C and held at each temperature for 1 h prior to the impedance measurements. The AC applied voltage was 100 mV.

3. Results and discussion

Fig. 1a and b show the XRD patterns of the SEs of $Li_{6-2x}Ca_x$-PS_5Cl and $Li_{5.94}M_{0.06/n}{}^nPS_5Cl$ ($M^n = Mg^{2+}$, Ba^{2+}, Zn^{2+}, Al^{3+}, Y^{3+}), respectively. No impurity was detected, and all the peaks were assignable to the argyrodite phase (JCPDS 34-0688). The lattice constant, interplanar spacing, and micro-strain were calculated using the XRD data to investigate the effect of the multivalent cation substitution on the crystal structure of Li_6PS_5Cl. The crystal structure of the samples was indexed to cubic Li_7PS_6 in the $F\bar{4}3m$ space group (JCPDS 34-0688). The peaks were assigned to the [111], [200], [220], [311], [222], [420], [422], [511], [440], [600], and [620] planes. The lattice parameters were obtained at each diffraction angle (θ) using the Bragg equation.

$$n\lambda = 2d\sin\theta. \quad (1)$$

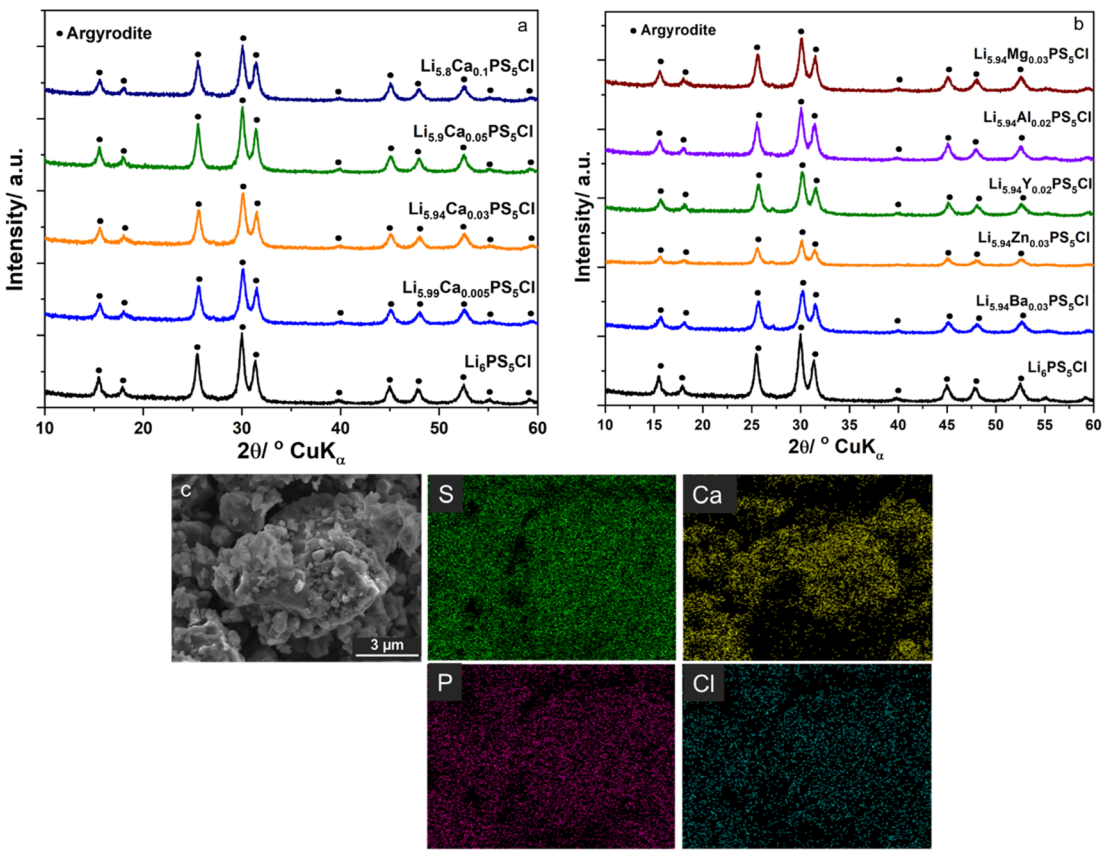

Fig. 1 Structural characterization of the prepared samples. (a) XRD patterns of $Li_{6-2x}Ca_xPS_5Cl$ solid electrolytes; (b) XRD patterns of $Li_{5.94}M_{0.06/n}{}^nPS_5Cl$ solid electrolytes ($M^n = Mg^{2+}$, Ba^{2+}, Zn^{2+}, Al^{3+}, Y^{3+}); (c) SEM-EDS results of $Li_{5.8}Ca_{0.1}PS_5Cl$.

Table 1 Structural parameters of the prepared samples

	Lattice constant a_0 (Å)	d_{220} (Å)	d_{311} (Å)	d_{222} (Å)	Microstrain ε
Li_6PS_5Cl	9.8401	3.4790	2.9669	2.8406	0.00330
$Li_{5.99}Ca_{0.005}PS_5Cl$	9.8400	3.4790	2.9669	2.8406	0.00418
$Li_{5.94}Ca_{0.03}PS_5Cl$	9.8346	3.4781	2.9661	2.8399	0.00433
$Li_{5.8}Ca_{0.1}PS_5Cl$	9.8341	3.4779	2.9660	2.8397	0.00390
$Li_{5.94}Ba_{0.03}PS_5Cl$	9.8347	3.4771	2.9653	2.8390	0.00460
$Li_{5.94}Zn_{0.03}PS_5Cl$	9.8348	3.4771	2.9653	2.8391	0.00458
$Li_{5.94}Mg_{0.03}PS_5Cl$	9.8356	3.4774	2.9655	2.8393	0.00488
$Li_{5.94}Al_{0.02}PS_5Cl$	9.8354	3.4778	2.9667	2.8404	0.00418
$Li_{5.94}Y_{0.02}PS_5Cl$	9.8349	3.4772	2.9653	2.8391	0.00445

$$\frac{1}{d^2} = \frac{h^2 + k^2 + l^2}{a^2}. \tag{2}$$

The Nelson–Riley equation was employed to determine the lattice constant (a_0).

$$a \approx \frac{1}{2}\left[\frac{\cos\theta^2}{\sin\theta} + \frac{\cos\theta^2}{\theta}\right]. \tag{3}$$

The a_0 was determined from the linear fit equation, which was derived from a plot with a as the y-axis and $\frac{1}{2}\left[\frac{\cos\theta^2}{\sin\theta} + \frac{\cos\theta^2}{\theta}\right]$ as the x-axis.

The Williamson–Hall (WH) analysis is a simple method for estimating the lattice strain (ε) by analyzing the X-ray data and considering the peak width as a function of 2θ.

$$\beta_{hkl}\cos\theta = 4\varepsilon\sin\theta + \frac{k\lambda}{d}, \tag{4}$$

where β_{hkl} is the full width at half maximum of the diffraction peak, and θ is the Bragg angle. The value of ε was derived from the slope of the regression line, which was obtained by plotting $\beta_{hkl}\cos\theta$ against $\sin\theta$.

Table 1 lists the values of the lattice constant (a_0), interplanar spacing (d_{220}, d_{311}, d_{222}), and micro-strain (ε). The a_0 of Li_6PS_5Cl was 9.8401 Å and was consistent with the reported 9.8397(4) Å of Li_6PS_5Cl prepared *via* the mechanochemical method.[16] The a_0 of

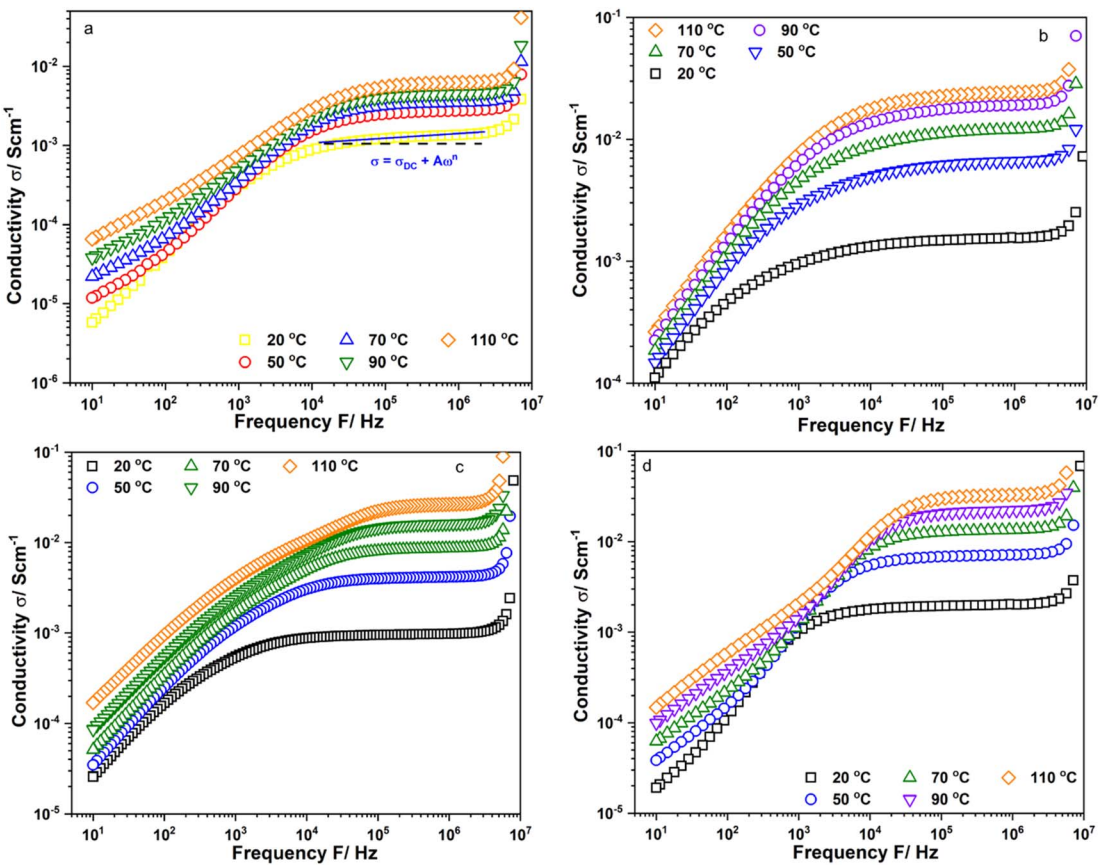

Fig. 2 Conductivity isotherms of (a) Li_6PS_5Cl; (b) $Li_{5.94}Ca_{0.03}PS_5Cl$; (c) $Li_{5.94}Mg_{0.03}PS_5Cl$ and (d) $Li_{5.94}Al_{0.02}PS_5Cl$ measured from 10 Hz to 9 MHz.

$Li_{5.99}Ca_{0.005}PS_5Cl$ was practically similar to that of Li_6PS_5Cl, indicating that the doping amount was too small to influence the measurement result. The a_0 of $Li_{5.94}Ca_{0.03}PS_5Cl$ was 9.8346 Å, which was smaller than that of Li_6PS_5Cl. The a_0 values of $Li_{5.94}M_{0.06/n}{}^nPS_5Cl$ ($M^n = Mg^{2+}$, Ca^{2+}, Ba^{2+}, Zn^{2+}, Al^{3+}, Y^{3+}) were close to each other. Thus, the multivalent cation doping reduced the a_0 of Li_6PS_5Cl; this observation was consistent with reported results.[11,12] The values of the interplanar spacing (d_{220}, d_{311}, d_{222}) of the substituted samples were smaller than those of Li_6PS_5Cl. In crystals, cations are surrounded by anions and *vice versa* such that the electrostatic interaction among oppositely charged ions strengthens the crystal structure. The substitution of Li ions with multivalent cations resulted in the formation of vacancies. A multivalent cation has a higher positive charge density than a Li ion; therefore, the electrostatic attraction with negative ions will be stronger. Thus, the lattice constant and interplanar spacing will be reduced. The lattice strain (ε) represents the displacement of unit cells about their normal positions. All the prepared samples exhibited a positive lattice strain, and the substituted samples exhibited higher strains than Li_6PS_5Cl. SEM-EDS results of $Li_{5.8}Ca_{0.1}PS_5Cl$ is shown in Fig. 1c. The SEs are in the form of particles with a size of several hundred nanometer. EDS results indicated that Ca was well dispersed in the prepared powder sample. The results suggest that the multivalent cations were successfully incorporated into the crystal structure of Li_6PS_5Cl.

Fig. 2a–d show the frequency dependence of the real part of conductivity, σ', of Li_6PS_5Cl, $Li_{5.94}Ca_{0.03}PS_5Cl$, $Li_{5.94}Mg_{0.03}PS_5Cl$, and $Li_{5.94}Al_{0.02}PS_5Cl$ obtained from 10 Hz to 9 MHz at different temperatures, respectively, using conductivity isotherms. Fig. S1a–c† show the conductivity isotherms of $Li_{5.96}Ca_{0.002}PS_5Cl$, $Li_{5.9}Ca_{0.05}PS_5Cl$, and $Li_{5.8}Ca_{0.1}PS_5Cl$, respectively. Furthermore, Fig. S2a–c† show the conductivity isotherms of $Li_{5.94}Ba_{0.03}PS_5Cl$, $Li_{5.94}Zn_{0.03}PS_5Cl$, and $Li_{5.94}Y_{0.02}PS_5Cl$, respectively. The isotherms of all the samples comprised three regions: electrode polarization, a plateau-like region, and polarization conductivity at low, intermediate, and high frequencies, respectively. The high-frequency polarization conductivity could be explained by the power law behavior, $\sigma_\omega \propto \omega^n$, where n is a fractional exponent ($0 \leq n \leq 1$) and is associated with the interaction between the ions and environment.[17] The accumulation of ions at blocking electrodes caused electrode polarization.[18] The isotherms were analyzed using the Jonscher power law to understand the ion dynamics of the prepared electrolytes. The conductivity in the intermediate- and high-frequency regions followed the Jonscher power law equation.

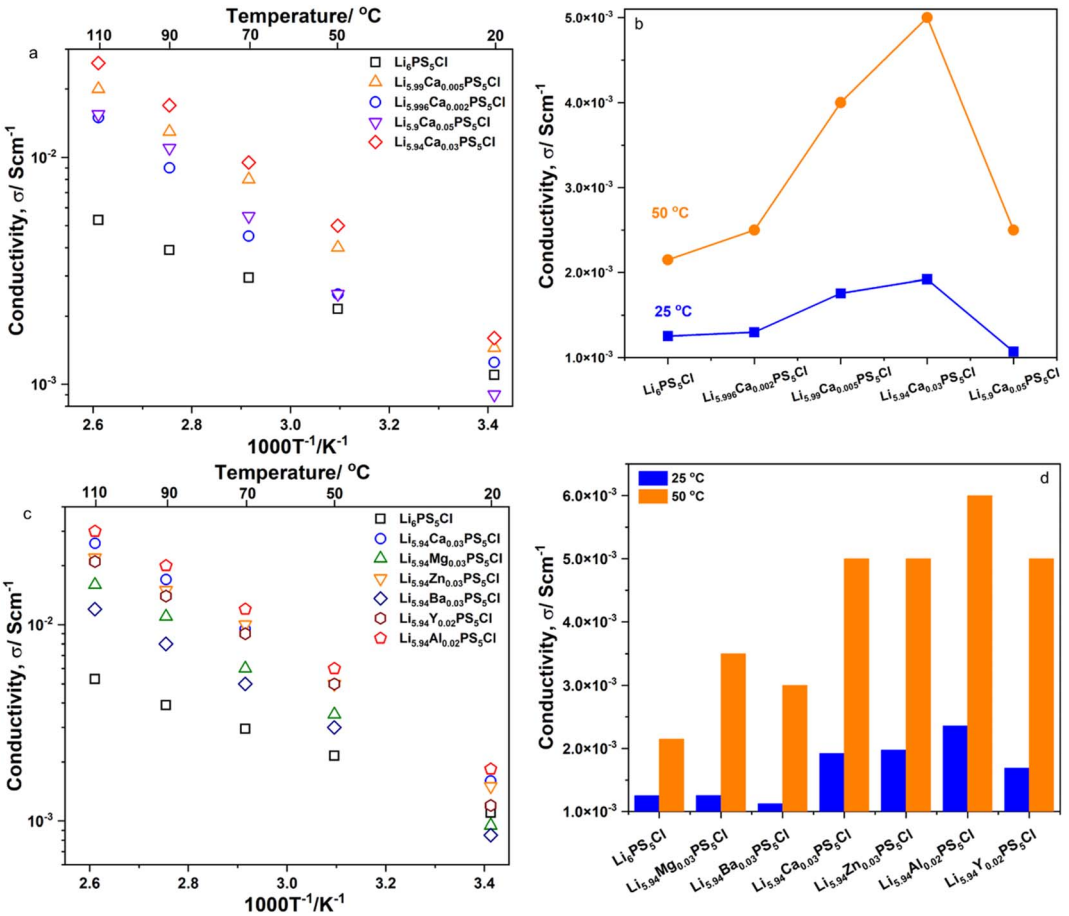

Fig. 3 (a) Temperature dependence of ionic conductivity of $Li_{6-2x}Ca_xPS_5Cl$ solid electrolytes; (b) the ionic conductivity at 25 and 50 °C of $Li_{6-2x}Ca_xPS_5Cl$ solid electrolytes; (c) temperature dependence of ionic conductivity of $Li_{5.94}M_{0.06/n}{}^nPS_5Cl$ solid electrolytes ($M^n = Mg^{2+}$, Ba^{2+}, Zn^{2+}, Al^{3+}, Y^{3+}); (d) the ionic conductivity at 25 and 50 °C of $Li_{5.94}M_{0.06/n}{}^nPS_5Cl$ solid electrolytes ($M^n = Mg^{2+}$, Ba^{2+}, Zn^{2+}, Al^{3+}, Y^{3+}).

$$\sigma = \sigma_{DC} + A\omega^n, \quad (5)$$

$$\rightarrow \sigma - \sigma_{DC} = A\omega^n \rightarrow \log_{10}(\sigma - \sigma_{DC}) = n\log_{10}\omega + \log_{10}A, \quad (6)$$

where σ_{DC} is the direct current (DC) conductivity, A is a pre-factor, and n is the frequency exponent in the range of $0 < n < 1$.[19] A and n are thermally activated quantities. σ_{DC}, A, and n were obtained at each temperature by fitting the conductivity spectra using eqn (6). Table 1 lists the values of A and n. All the values of A and n exceeded 0, indicating the frequency and temperature dependence of the conductivity. The A values of the doped samples were approximately 10^1 to 10^2 times that of Li_6PS_5Cl, suggesting that the multivalent cation doping enhanced the frequency dependence conductivity.

Fig. 3a and c show the temperature dependence of the ionic conductivity, σ_{DC}, of the SEs of $Li_{6-2x}Ca_xPS_5Cl$ and $Li_{5.94}M_{0.06/n}{}^nPS_5Cl$ (M^n = Mg^{2+}, Ba^{2+}, Zn^{2+}, Al^{3+}, Y^{3+}), respectively. The

Table 2 DC activation energy $E_{a,DC}$, activation energy $E_{a,m}$ of ion migration at grain boundary, and characteristic time $\tau_{0,m}$ of ion migration at grain boundary

	Li_6PS_5Cl	$Li_{5.96}Ca_{0.002}PS_5Cl$	$Li_{5.94}Ca_{0.03}PS_5Cl$	$Li_{5.9}Ca_{0.05}PS_5Cl$	$Li_{5.8}Ca_{0.1}PS_5Cl$
$E_{a,DC}$/kJ mol^{-1}	16	26	29	28	31
$E_{a,DC}$/eV	0.16	0.26	0.29	0.28	0.31
$E_{a,m}$/kJ mol^{-1}	19	24	28	31	34
$E_{a,m}$/eV	0.19	0.24	0.28	0.31	0.34
$\tau_{0,m}$/s	5.47×10^{-7}	2.56×10^{-9}	6.31×10^{-9}	1.57×10^{-9}	6.79×10^{-9}
	$Li_{5.94}Ba_{0.03}PS_5Cl$	$Li_{5.94}Zn_{0.03}PS_5Cl$	$Li_{5.94}Mg_{0.03}PS_5Cl$	$Li_{5.94}Al_{0.02}PS_5Cl$	$Li_{5.94}Y_{0.02}PS_5Cl$
$E_{a,DC}$/kJ mol^{-1}	27	28	29	29	29
$E_{a,DC}$/eV	0.27	0.28	0.29	0.29	0.29
$E_{a,m}$/kJ mol^{-1}	31	31	31	33	30
$E_{a,m}$/eV	0.31	0.31	0.31	0.33	0.30
$\tau_{0,m}$/s	8.66×10^{-9}	1.39×10^{-9}	4.42×10^{-9}	2.26×10^{-9}	1.64×10^{-9}

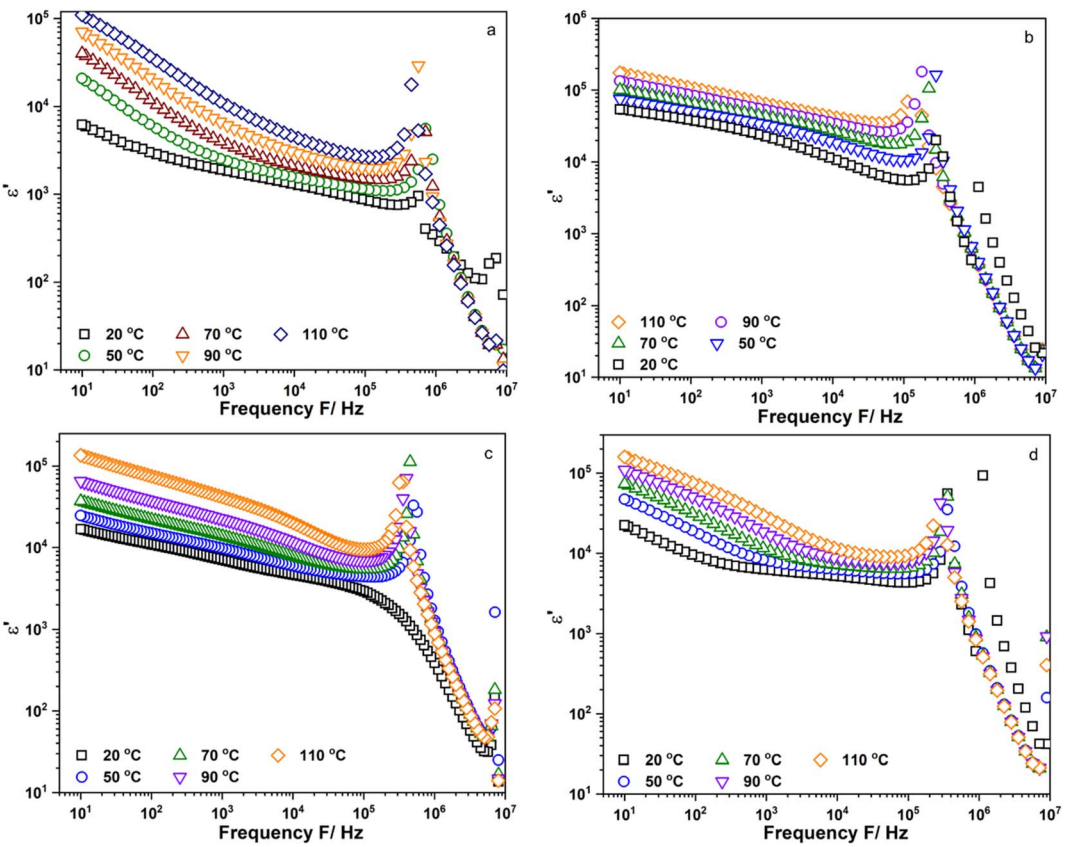

Fig. 4 Frequency dependent of the real part of permittivity, ε′, of (a) Li_6PS_5Cl; (b) $Li_{5.94}Ca_{0.03}PS_5Cl$; (c) $Li_{5.94}Mg_{0.03}PS_5Cl$ and (d) $Li_{5.94}Al_{0.02}PS_5Cl$ measured from 10 Hz to 9 MHz.

$\log_{10}(\sigma_{DC})$ satisfied a practically linear dependence on an inverse temperature; therefore, it followed the Arrhenius equation, $\sigma = \sigma_0 \exp(-E_{a,DC}/(k_B T))$. The DC activation energy, $E_{a,DC}$, was calculated and is shown in Table 2. The $E_{a,DC}$ of Li_6PS_5Cl was approximately 16 kJ mol^{-1}. The $E_{a,DC}$ of the doped samples exceeded that of Li_6PS_5Cl in the range of 28–31 kJ mol^{-1}. Furthermore, the $E_{a,DC}$ of $Li_{6-3x}Al_xPS_5Br$ ($x = 0.1$, 0.15, 0.2, 0.25, 0.3) has been reported to exceed that of Li_6PS_5Br.[12] Thus, the aliovalent substitution of Li ions in argyrodite-type SEs led to an increase in $E_{a,DC}$. The ionic conductivity of Li_6PS_5Cl at 25 °C was approximately 1.25×10^{-3} S cm^{-1}. Fig. 3b and d show the ionic conductivity (σ_{DC}) of the SEs of $Li_{6-2x}Ca_xPS_5Cl$ and $Li_{5.94}M_{0.06/n}{}^nPS_5Cl$ ($M^n = Mg^{2+}$, Ba^{2+}, Zn^{2+}, Al^{3+}, Y^{3+}) at 25 °C and 50 °C, respectively. At 25 °C, all the doped samples exhibited ionic conductivities higher than that of Li_6PS_5Cl. $Li_{5.94}Al_{0.02}PS_5Cl$ exhibited the highest σ_{DC} (approximately 2.36×10^{-3} S cm^{-1}) at 25 °C. The σ_{DC} of Li_6PS_5Cl and $Li_{5.94}Al_{0.02}PS_5Cl$ were 2.15×10^{-3} and 6.00×10^{-3} S cm^{-1} at 50 °C, respectively. The σ_{DC} and $E_{a,DC}$ results confirmed that the multivalent cation was successfully incorporated into the crystal structure of Li_6PS_5Cl.

Fig. 4a–d show the frequency dependence of the real part of permittivity, ε', of Li_6PS_5Cl, $Li_{5.94}Ca_{0.03}PS_5Cl$, $Li_{5.94}Mg_{0.03}PS_5Cl$, and $Li_{5.94}Al_{0.02}PS_5Cl$ obtained from 10 Hz to 9 MHz at different temperatures, respectively. Fig. S3a–c† show the frequency dependence of the ε' of $Li_{5.96}Ca_{0.002}PS_5Cl$, $Li_{5.9}Ca_{0.05}PS_5Cl$, and $Li_{5.8}Ca_{0.1}PS_5Cl$, respectively. Furthermore, Fig. S4a–c† show the frequency dependence of the ε' of $Li_{5.94}Ba_{0.03}PS_5Cl$, $Li_{5.94}Zn_{0.03}PS_5Cl$, and $Li_{5.94}Y_{0.02}PS_5Cl$, respectively. The increase in the plots in the low-frequency region was attributable to the electrode–electrolyte interface polarization due to the accumulation of ions near the electrode. This led to the formation of a space-charged layer that blocked the electric field and enhanced the electrical polarization. The ε' of all the samples increased with an increase in temperature, indicating that charge carrier movement was thermally activated. The ε' reflects the amount of energy stored in the form of polarization when an electric field is applied.[20] In most ion-conducting materials, ε' decreases with an increase in frequency.[21] The plot of $Li_{5.94}Mg_{0.03}PS_5Cl$ at room temperature continuously decreased in the intermediate- and high-frequency regions; however, the plots of the other samples obtained at room temperature exhibited maxima at 10^5–10^6 Hz. Maxima were observed in all the plots at 50 °C or above. The change in the shape of the plots of $Li_{5.94}Mg_{0.03}PS_5Cl$ suggests that a change occurred in the microstructure, and this process was temperature-dependent.

Fig. 5a–d show the frequency dependence of the loss factor, tan δ, of Li_6PS_5Cl, $Li_{5.94}Ca_{0.03}PS_5Cl$, $Li_{5.94}Mg_{0.03}PS_5Cl$, and $Li_{5.94}Al_{0.02}PS_5Cl$ obtained from 10 Hz to 9 MHz at different temperatures, respectively. Fig. S5a–c† show the frequency

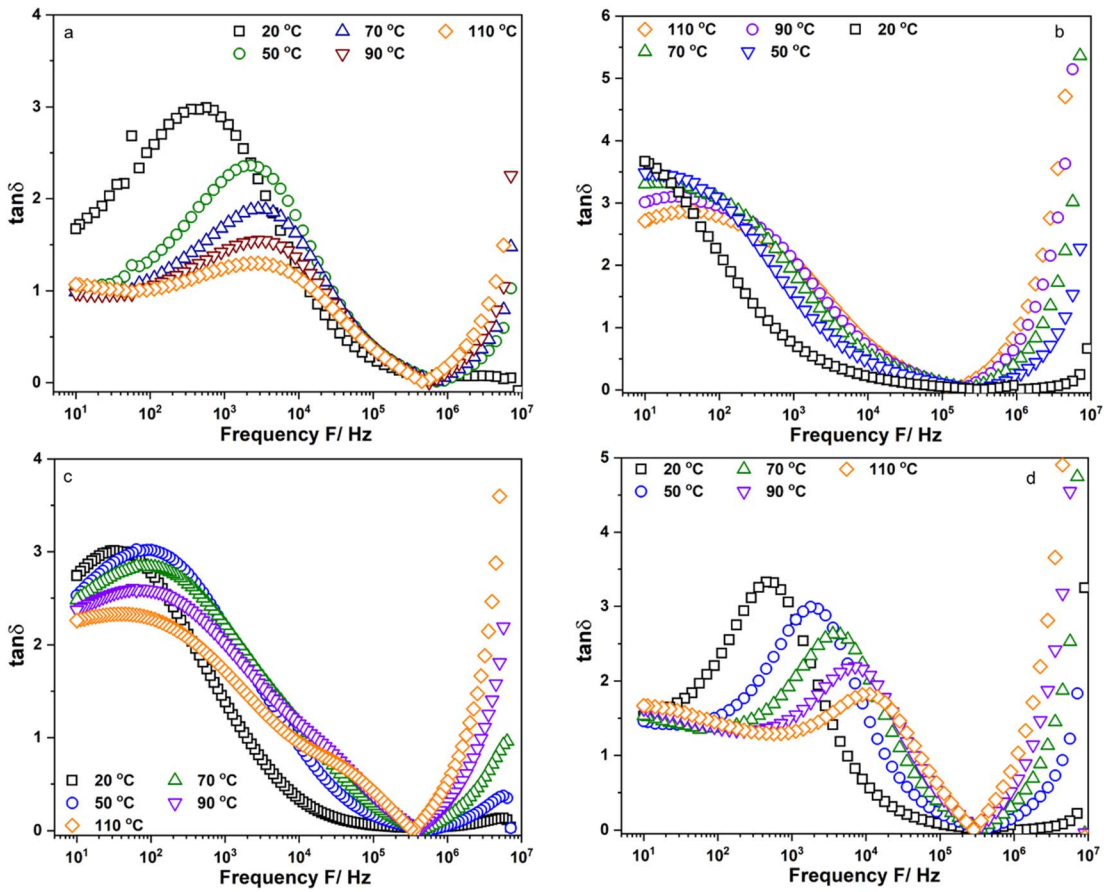

Fig. 5 Frequency dependent of the loss factor, tan δ, of (a) Li_6PS_5Cl; (b) $Li_{5.94}Ca_{0.03}PS_5Cl$; (c) $Li_{5.94}Mg_{0.03}PS_5Cl$ and (d) $Li_{5.94}Al_{0.02}PS_5Cl$ measured from 10 Hz to 9 MHz.

dependence of the tan δ of $Li_{5.96}Ca_{0.002}PS_5Cl$, $Li_{5.9}Ca_{0.05}PS_5Cl$, and $Li_{5.8}Ca_{0.1}PS_5Cl$, respectively. Fig. S6a–c† show the frequency dependence of the tan δ of $Li_{5.94}Ba_{0.03}PS_5Cl$, $Li_{5.94}Zn_{0.03}PS_5Cl$, and $Li_{5.94}Y_{0.02}PS_5Cl$, respectively. Two peaks assignable to ion migration at the grain boundary and bulk were observed in all the plots in the low- and high-frequency regions. The peak in the low-frequency region shifted toward high-frequency with an increase in temperature. Generally, the grain boundary migration resistivity was expected to decrease with an increase in temperature because Li^+ diffused from the bulk to the grain boundary. Thus, the intensity of the peak corresponding to the grain boundary resistivity in the loss factor decreased with an increase in temperature. The peak in the high-frequency region was not fully observed at 50 °C or above. The maximum value of the peak in the high-frequency region increased with an increase in the temperature, indicating that the number of charge carriers increased because of thermal activation. The migration energy ($E_{a,m}$) and migration characteristic time ($\tau_{0,m}$) of the Li^+ moving at the grain boundary could be derived from the temperature dependence of the peak position at low-frequency in the tan δ using the Arrhenius equation, $\tau_m = \tau_{0,m}\exp(-E_{a,m}/(k_BT))$. Table 2 lists the obtained $E_{a,m}$ and $\tau_{0,m}$ values. The $E_{a,m}$ of the samples was similar to the $E_{a,DC}$, implying that the ion migration at the grain boundary was a critical process. The $\tau_{0,m}$ of Li_6PS_5Cl was approximately 5.47×10^{-7} s. The $\tau_{0,m}$ of the doped samples was approximately 10^{-9} s, which was almost 10^2 times faster than that of Li_6PS_5Cl. Thus, the Li ion moving at the grain boundary changed from long-range diffusion in Li_6PS_5Cl to short-range diffusion in the doped samples. The results suggested that the substitution of the Li ion with multivalent cations resulted in vacancy formation, which was the new hopping position for the Li ion. The addition of multivalent ions to Li_6PS_5Cl enhanced the Li ion mobility with a gradual decrease in the migration time; however, the migration energy increased as reflected in the $E_{a,m}$. Multivalent cations have a higher positive charge than Li^+; thus, Li ions are repelled from their vicinity. From there, an Li ion can be trapped near the multivalent ion site, leading to a high migration barrier. It has been reported that the short inter-cage jump is a critical process in $Li_{5.4}Al_{0.2}PS_5Br$, and this process was associated with an increase in activation energy.[12] In addition, the change from short- to long-range diffusion was associated with a decrease and increase in activation energy and migration time, respectively.[22] Thus, the results in this section were consistent with the reported results and ionic conductivity of the samples.

4. Conclusion

Here, the Li ion in the SE of Li_6PS_5Cl was partially substituted with various multivalent cations (Mg^{2+}, Ba^{2+}, Zn^{2+}, Al^{3+}, Y^{3+}). The a_0; d_{220}, d_{311}, d_{222}; ε; and σ_{DC} values confirmed that the multivalent cations were successfully incorporated into the crystal structure of Li_6PS_5Cl. In addition, the charge carrier movement at the grain boundary changed from long-range diffusion in Li_6PS_5Cl to short-range diffusion in the doped samples.

Conflicts of interest

The authors declare that they have no known competing financial interests or personal relationships that could have appeared to influence the work reported in this paper.

Acknowledgements

We acknowledge Ho Chi Minh City University of Technology (HCMUT), VNU-HCM for supporting this study. The authors thank Philip K. (Enago; https://www.enago.com/vnuhcm/) for the English language review.

References

1 Y. Kato, S. Hori, T. Saito, K. Suzuki, M. Hirayama, A. Mitsui, M. Yonemura, H. Iba and R. Kanno, High-power all-solid-state batteries using sulfide superionic conductors, *Nat. Energy*, 2016, **1**, 16030.

2 F. Mizuno, A. Hayashi, K. Tadanaga and M. Tatsumisago, New, Highly Ion-Conductive Crystals Precipitated from Li_2S–P_2S_5 Glasses, *Adv. Mater.*, 2005, **17**, 918–921.

3 N. Kamaya, K. Homma, Y. Yamakawa, M. Hirayama, R. Kanno, M. Yonemura, T. Kamiyama, Y. Kato, S. Hama, K. Kawamoto and A. Mitsui, A lithium superionic conductor, *Nat. Mater.*, 2011, **10**, 682–686.

4 Y. Subramanian, R. Rajagopal and K.-S. Ryu, Synthesis of Sb-doped $Li_{10}P_3S_{12}I$ solid electrolyte and their electrochemical performance in solid-state batteries, *J. Energy Storage*, 2024, **78**, 2717–2728.

5 L. Zhou, N. Minafra, W. G. Zeier and L. F. Nazar, Innovative Approaches to Li-Argyrodite Solid Electrolytes for All-Solid-State Lithium Batteries, *Acc. Chem. Res.*, 2021, **54**, 2717–2728.

6 T. T. Zuo, F. Walther, J. H. Teo, R. Ruess, Y. Wang, M. Rohnke, D. Schroder, L. F. Nazar and J. Janek, Impact of the Chlorination of Lithium Argyrodites on the Electrolyte/Cathode Interface in Solid-State Batteries, *Angew Chem. Int. Ed. Engl.*, 2023, **62**, e202213228.

7 P. Adeli, J. D. Bazak, K. H. Park, I. Kochetkov, A. Huq, G. R. Goward and L. F. Nazar, Boosting Solid-State Diffusivity and Conductivity in Lithium Superionic Argyrodites by Halide Substitution, *Angew Chem. Int. Ed. Engl.*, 2019, **58**, 8681–8686.

8 Y. Subramanian, R. Rajagopal, S. Kang and K.-S. Ryu, Optimization of high ionic conducting Br-rich and metal (Sb and Zr) substituted Li-argyrodite and their enhanced air stability and compatibility in lithium batteries, *Scr. Mater.*, 2023, **235**, 115592.

9 J. Lin, G. Cherkashinin, M. Schäfer, G. Melinte, S. Indris, A. Kondrakov, J. Janek, T. Brezesinski and F. Strauss, A High-Entropy Multicationic Substituted Lithium Argyrodite Superionic Solid Electrolyte, *ACS Mater. Lett.*, 2022, **4**, 2187–2194.

10 Y. Subramanian, R. Rajagopal, B. Senthilkumar, Y. J. Park, S. Kang, Y. J. Jung and K.-S. Ryu, Tuning of Li-argyrodites ionic conductivity through silicon substitution ($Li_{6+x}P_{1-x}Si_xS_5Cl_{0.5}Br_{0.5}$) and their electrochemical performance in

lithium solid state batteries, *Electrochim. Acta*, 2021, **400**, 139431.

11 P. Adeli, J. D. Bazak, A. Huq, G. R. Goward and L. F. Nazar, Influence of Aliovalent Cation Substitution and Mechanical Compression on Li-Ion Conductivity and Diffusivity in Argyrodite Solid Electrolytes, *Chem. Mater.*, 2020, **33**, 146–157.

12 Z. Zhang, J. Zhang, H. Jia, L. Peng, T. An and J. Xie, Enhancing ionic conductivity of solid electrolyte by lithium substitution in halogenated Li-argyrodite, *J. Power Sources*, 2020, **450**, 227601.

13 T. Asano, A. Sakai, S. Ouchi, M. Sakaida, A. Miyazaki and S. Hasegawa, Solid Halide Electrolytes with High Lithium-Ion Conductivity for Application in 4 V Class Bulk-Type All-Solid-State Batteries, *Adv. Mater.*, 2018, **30**, e1803075.

14 K. Hikima, N. H. Huy Phuc, H. Tsukasaki, S. Mori, H. Muto and A. Matsuda, High ionic conductivity of multivalent cation doped Li_6PS_5Cl solid electrolytes synthesized by mechanical milling, *RSC Adv.*, 2020, **10**, 22304–22310.

15 N. H. H. Phuc, M. Totani, K. Morikawa, H. Muto and A. Matsuda, Preparation of Li_3PS_4 solid electrolyte using ethyl acetate as synthetic medium, *Solid State Ionics*, 2016, **288**, 240–243.

16 S. Boulineau, M. Courty, J.-M. Tarascon and V. Viallet, Mechanochemical synthesis of Li-argyrodite Li_6PS_5X (X=Cl, Br, I) as sulfur-based solid electrolytes for all solid state batteries application, *Solid State Ionics*, 2012, **221**, 1–5.

17 K. P. Padmasree and A. F. Fuentes, Dielectric relaxation studies of $Ce_{0.9-x}Y_xCa_{0.1}O_{2-\delta}$ solid electrolytes, *Mater. Chem. Phys.*, 2019, **223**, 466–472.

18 F. Preishuber-Pflugl and M. Wilkening, Mechanochemically synthesized fluorides: local structures and ion transport, *Dalton Trans.*, 2016, **45**, 8675–8687.

19 A. K. Jonscher, The 'Universal' dielectric response, *Nature*, 1977, **267**, 673–679.

20 D. M. Abdel Basset, S. Mulmi, M. S. El-Bana, S. S. Fouad and V. Thangadurai, Synthesis and characterization of novel Li-stuffed garnet-like $Li_{5+2x}La_3Ta_{2-x}Gd_xO_{12}$ ($0 \leq x \leq 0.55$): structure-property relationships, *Dalton Trans.*, 2017, **46**, 933–946.

21 A. A. Ibrahim, D. A. Kospa, O. R. Hayes, A. S. Khder, S. A. El-Hakam and A. I. Ahmed, Cesium salt of tungstophosphoric acid/mesoporous (zirconia-silica) composite for highly efficient synthesis of 7-hydroxy-4-methyl coumarin and removal of methylene blue, *RSC Adv.*, 2023, **13**, 15243–15260.

22 T. A. Tu, T. V. Toan, L. T. Anh, L. V. Thang and N. H. H. Phuc, Synergic effect of CaI_2 and LiI on ionic conductivity of solution-based synthesized $Li_7P_3S_{11}$ solid electrolyte, *RSC Adv.*, 2024, **14**, 5764–5770.